Internal polarization dynamics of vector dissipative-soliton-resonance pulses in normal dispersion fiber lasers

Daojing Li,[1,3] Deyuan Shen,[1] Lei Li,[2] Dingyuan Tang,[2] Lei Su,[4] and Luming Zhao[2,5,*]

[1]*Department of optical science and engineering, Fudan University, Shanghai 200433, China*

[2]*Jiangsu Key Laboratory of Advanced Laser Materials and Devices, Jiangsu Collaborative Innovation Center of Advanced Laser Technology and Emerging Industry, School of Physics and Electronic Engineering, Jiangsu Normal University, Xuzhou, Jiangsu 221116 China*

[3]*Optical Sciences Group, Research School of Physics and Engineering, The Australian National University, Canberra ACT 2600, Australia*

[4]*School of Engineering and Materials Science, Queen Mary University of London, London, UK*

[5]*Key Laboratory of Optoelectronic Devices and Systems of Ministry of Education and Guangdong Province, Shenzhen University, 518060, China*

(Dated: February 7, 2018)

Abstract

Internal polarization dynamics of vector dissipative-soliton-resonance (DSR) pulses in a mode-locked fiber laser is investigated. By utilizing a waveplate-analyzer configuration to analyze the special structure of a DSR pulse, we find that polarization state is not uniform across a resonant dissipative soliton. Specifically, although the central plane wave of the resonant dissipative soliton acquires nearly a single fixed polarization, the dissipative fronts feature polarization states that are different and spatially varying. This distinct polarization distribution is maintained while the whole soliton extends with increasing gain. Numerical simulation further confirms the experimental observations.

Dissipative solitons (DS) appear widely in physical, biological, and medical systems with the presence of continuous energy or matter supply and dissipation [1]. An important aspect of the concept of the DS is that it extends soliton theory from nonlinear integrable systems to dissipative systems and promotes the generation of ultrafast optical pulses in mode-locked fiber lasers with unprecedented energy levels [2]. Particularly, a recently developed approach known as the dissipative-soliton-resonance (DSR) effect [3], provides the possibility of avoiding pulse break-up and has boosted pulse energy impressively to tens of microjoules [4].

Apart from the capacity for fairly large energy pulse generation, resonant DSs (also referred to as DSR pulses, interchangeably), also demonstrate distinctive behaviours of strong physical interest. A DSR pulse is a complex of two interacting dissipative fronts. Under small-gain conditions, two fronts are closely connected, forming a plain DS. With increasing gain, the resonance effect limits the growth of peak power, while allows for two fronts moving apart from each other. The pulse generates a plane wave in the center, which strongly binds two fronts together. The central plane wave extends, and the distance between the two fronts grows linearly and infinitely with energy supply, whereas the fronts themselves do not change. The central plane wave and the fronts were also found to feature different chirps: a moderately low linear chirp throughout the extended central plane wave and large linear chirps across both fronts [5–8].

Here we carry out further research on internal polarization dynamics of the DSR pulse, taking into account its vector nature. Single-mode fibers are always weakly birefringent. Solitons thereby degenerate into two orthogonally-polarized components. There is a rich variety of vector soliton dynamics that has been analysed in optical fibers and mode-locked fiber lasers [9–12]. Sergeyev and co-authors have studies the stability and evolution of vector DSs at a time interval from a few to thousands of cavity round trips using a polarimeter [13, 14]. However, few insights into the internal polarization dynamics of DSs have been given. The duration of a plain DS in a fiber laser ranges typically from femtoseconds to several tens of picoseconds. Given the speed limitation of optical polarimeters, it is very challenging to gain insight into the internal polarization dynamics of such a short soliton. In this paper, we reveal the internal polarization dynamics of a DS for the first time, by utilizing a waveplate-analyzer configuration to analyze the special structure of a DSR pulse. The resonance effect also allows longer soliton duration, which facilitates the

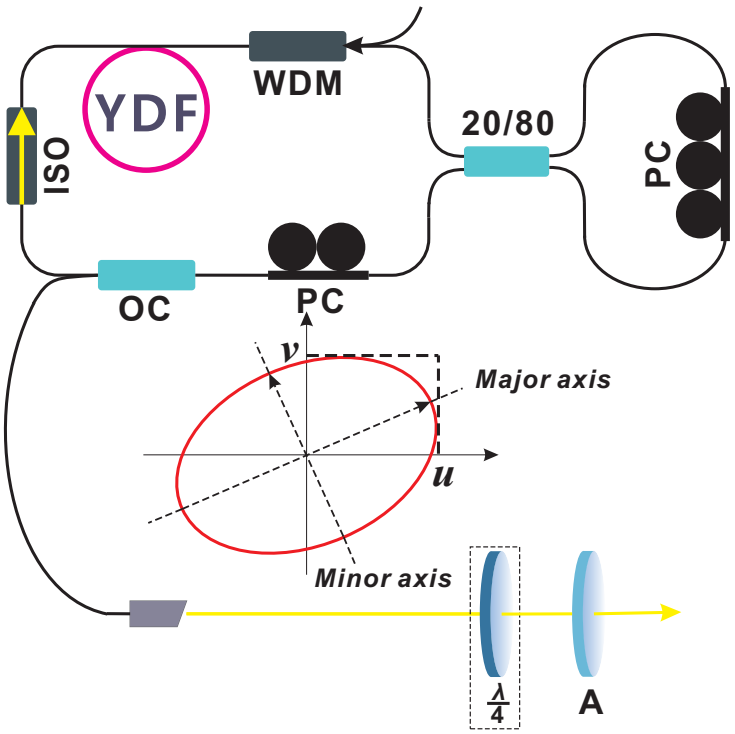

FIG. 1. Schematic of the laser setup. WDM: wavelength division multiplexer; ISO: isolator; PC: polarization controller; YDF: ytterbium-doped fiber; SMF: single-mode fiber; OC: output coupler; $\frac{\lambda}{4}$: quarter-wave plate; A: analyzer.

investigation of the internal dynamics. Experimental results show that the central plane wave of the resonant DS acquires nearly a single fixed state of polarization (SOP). However, the fronts feature different and spatially-varying SOP. This distinct polarization distribution is maintained while the whole soliton structure expands with increasing gain. Numerical simulation confirms the experiment.

Figure 1 shows the laser setup. A 42 cm ytterbium-doped fiber (YDF) was counter-pumped by a 976 nm laser diode. A polarization-independent isolator ensures unidirectional operation. A nonlinear optical loop mirror, formed by a 80:20 coupler and a 7-meter-long SMF, provides saturable absorption. The split ratio of the coupler and the length of loop were chosen so as to ensure strong peak-power-clamping effect, which is crucial for achieving DSR [6]. Two polarization controllers (PCs) were used, providing careful optimization of the cavity birefringence. The total cavity length is 13.6 m, corresponding to a repetition frequency of 15.2 MHz. The estimated total cavity dispersion is 0.30 ps^2. A 30% coupler provides laser output. A high-speed photodetector-oscilloscope combination

with a bandwidth of 45 GHz is used to monitor the output.

By appropriate adjustment of the PCs, resonant DSs could be easily obtained in the laser. The pulse evolves to a flat top profile with increasing pump [see Fig. 2(a)]. Pulse duration and energy show linear growth with the pump power [see Fig. 2(b)]; these are typical DSR features. Moreover, the radio frequency spectrum shows a high contrast of more than 60 dB [see Fig. 2(c)]. The resolution bandwidth of the RF spectrum analyzer was set at 10 Hz. We realize that noise-like pulses in mode-locked fiber laser can also feature flat top profile with tunable pulse width [15, 16]. A crucial feature that distinguishes the obtained DSR pulse here from noise-like pulses is its spectral behavior. Noise-like pulses exhibit relatively smooth profiles without any fine internal structure. However, the spectrum of the obtained DSR pulse, as shown in Fig. 2(d), has steep edges and the same behaviour with gain variation as was found in [7]. Thus, with increasing pump, the newly-emerging spectrum appears at the center and forms a spike, while its rectangular pedestal remains unchanged.

For polarization-resolved measurements, the laser output was connected to a collimator and then passed through a rotatable analyzer. The axis of the analyzer was aligned to the maximum (minimum) of the energy transmission, thus obtaining the major (minor) component of the pulse. We set a proper pump power of 350 mW and conducted the polarization-resolved measurement. The original pulse duration is 300 ps [see purple dot-dashed line in Fig. 2(a)]. The ratio between maximal and minimal transmitted energy measured is around 12:1, indicating that the resonant pulse is elliptically polarized, i.e. it is a vector soliton. Results of polarization-resolved measurement are summarized in the rest of Fig. 2. No wavelength shifting between two components is observed, suggesting a small cavity birefringence. Two components show no evolution in pattens through roundtrips [see Fig. 2(f)]. The radio frequency spectra of the components also show no polarization evolution frequency [10].

To obtain more insight into the internal polarization properties of the DSR pulses, we inserted a quarter-wave plate before the rotating analyzer. We recall that for an elliptically-polarized light wave, its resolved components along the major and minor axes have a phase difference of $\pm\pi/2$. When the light wave passes through a quarter-wave plate, if the fast (or slow) axis of the quarter-wave plate is parallel to one of the principal axes of the incident light, the quarter-wave plate will induce a phase shift of $\pm\pi/2$ between the two components. The resulting phase shift between the major and minor components then becomes 0 or $\pm\pi$.

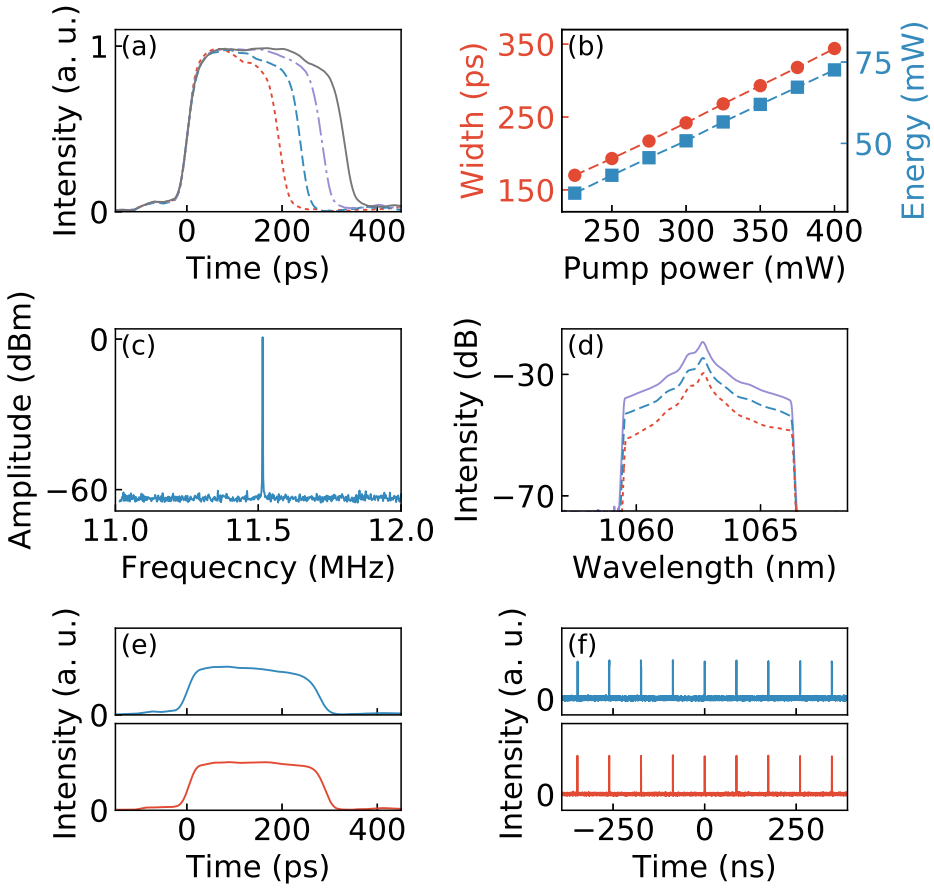

FIG. 2. (a) Single pulse traces as a function of increasing pump power: 250, 300, 350, and 400 mW. (b) Pulse energy (blue square), width (red dot) versus increasing pump power. (c) Radio frequency spectrum. (d-f) Polarization-resolved measurements of the pulse under pump power of 350 mW . (d) Spectra of original pulse (purple solid), major component (blue dashed), minor component (red dotted). (e) Single pulse traces and (f) pulse trains of the major component (top row) and minor component (bottom row).

Thus, the elliptically-polarized light will be converted to linearly-polarized light, which then can be blocked by a rotating polarizer at a certain angle.

Accordingly, we used the waveplate-analyzer combination to test polarization dynamics of the DSR pulse, as depicted in Fig 1. The axis of the analyzer was first set to match the minor axis of the DSR pulse by identifying the minimal energy transmission. Then a quarter-wave plate was inserted before the analyzer, with its fast axis carefully aligned parallel to the axis of the analyzer, therefore, parallel to the minor axis of the DSR pulse. Experimentally, we kept monitoring the transmitted light field while carefully rotating the

analyzer. Traces *i*-*k* in Fig. 3(a) show different states with a continuously rotating axis of the analyzer in the vicinity of the minimal light transmission. It turns out that the central plane wave of the DSR pulse rises or falls together with the rotating analyzer, whereas the two fronts present asymmetric oscillatory structures. Eventually, the central part would decrease to almost zero. However, the fronts would not do this, as one can see from trace *k* in Fig. 3(a). It looks as if the fronts form two separated pulses. Rotating the analyzer further away from state *k*, the central plane wave part started to rise back, while the fronts, after a short decrease, also began to rise. Surprisingly, the pulse as a whole could not be totally blocked by the analyzer.

The observation clearly suggests that the DSR pulse does not acquire a single SOP. The SOP of the fronts differs from that of the central plane wave: the central plane wave acquires a single fixed elliptical polarization, whereas the fronts have spatially-varying polarization. Since the central plane wave part makes up the majority of the whole structure, when we experimentally aligned the axis of the analyzer at the angle of the minimal energy transmission, we approximately identified the minor axis of the central plane wave. Therefore, when the pulse then passed through the quarter-wave plate, only the central plane wave part was converted to linearly-polarized light. However, because the SOP of the fronts was different and spatially-varying, the fronts could not be converted to linearly-polarized light. As a result, when the pulse was finally analyzed by the analyzer, only the central plane wave could be fully blocked, whereas the fronts ended up as two separated oscillatory waves.

The behaviour of the DSR pulse as pump power changes was also investigated. Fixing the set-up at state *k*, we only changed the pump power. The distance between two fronts varied linearly with changes in the pump power. Figure. 3(b) shows typical results with pump powers of 300, 350, 400 mW. After the waveplate-analyzer, the extended central plane wave was always blocked, whereas two fronts show only small fluctuations. The plane wave and fronts both maintain their unique polarization dynamics. Tuning the cavity PC settings, other DSR operation states can be observed in the cavity. All the states show similar SOP distributions.

The experiment reveals that the vector soliton under DSR exhibits a non-uniform polarization distribution across the whole structure. To confirm this, we performed numerical simulation on light circulation in the laser cavity. Pulse propagation through the fiber section is described by coupled Ginzburg-Landau equations having the form:

$$\frac{\partial u}{\partial z} = i\beta u - \sigma\frac{\partial u}{\partial t} - i\frac{k_2}{2}\frac{\partial^2 u}{\partial t^2} + i\frac{k_3}{6}\frac{\partial^3 u}{\partial t^3} + i\gamma\left(|u|^2 + \frac{2}{3}|v|^2\right)u + i\frac{\gamma}{3}v^2u^* + \frac{g}{2}u + \frac{g}{2\Omega_g^2}\frac{\partial^2 u}{\partial t^2} \tag{1a}$$

$$\frac{\partial v}{\partial z} = -i\beta v + \sigma\frac{\partial v}{\partial t} - i\frac{k_2}{2}\frac{\partial^2 v}{\partial t^2} + i\frac{k_3}{6}\frac{\partial^3 v}{\partial t^3} + i\gamma\left(|v|^2 + \frac{2}{3}|u|^2\right)v + i\frac{\gamma}{3}u^2v^* + \frac{g}{2}v + \frac{g}{2\Omega_g^2}\frac{\partial^2 v}{\partial t^2} \tag{1b}$$

where u and v are the slowly-varying envelopes of the two linearly-polarized components along the slow and fast polarization axes of the optical fiber, respectively. Here 2β is the wave-number difference, 2σ is the inverse group velocity difference, k_2, k_3, γ represent the second-order, third-order dispersion and Kerr nonlinearity of the fibers, g is the saturable gain of the YDF and Ω_g is the gain bandwidth. A parabolic gain shape, with 40 nm bandwidth, was assumed. The gain saturation was also considered for YDF

$$g = G_0 \exp\left[-\int\left(|u|^2 + |v|^2\right)dt/E_{sat}\right] \tag{2}$$

where G_0 is the small signal gain coefficient and E_{sat} is the saturation energy. The saturable absorption of the NOLM was modeled by its transmission function [17]

$$T = 1 - 2\alpha\left\{1 + \cos\left[(1-2\alpha)\gamma L\left(|u|^2 + |v|^2\right)\right]\right\} \tag{3}$$

where $\alpha = 0.2$ is the split ratio of the coupler. L is the loop length of 7 m. To potentially match with the experimental conditions, we set the parameters as follows: $k_2 = 22\ ps^2/km$, $k_3 = 0.1\ ps^3/km$, $\gamma = 5.8\ (W \cdot km)^{-1}$, $G_0 = 6.9\ m^{-1}$, $E_{sat} = 5\ nJ$. Considering a weak birefringence cavity, the beat length of the fiber was set to 5 m. The numerical model was solved by the split-step Fourier method. The same stable solutions were reached when using different initial conditions.

A convenient way to analyse the polarization dynamics is to use the Stokes parameters, defined as

$$S_0 = |u|^2 + |v|^2, S_1 = |u|^2 - |v|^2,$$
$$S_2 = 2|u||v|cos\Delta\psi, S_3 = 2|u||v|sin\Delta\psi \tag{4}$$

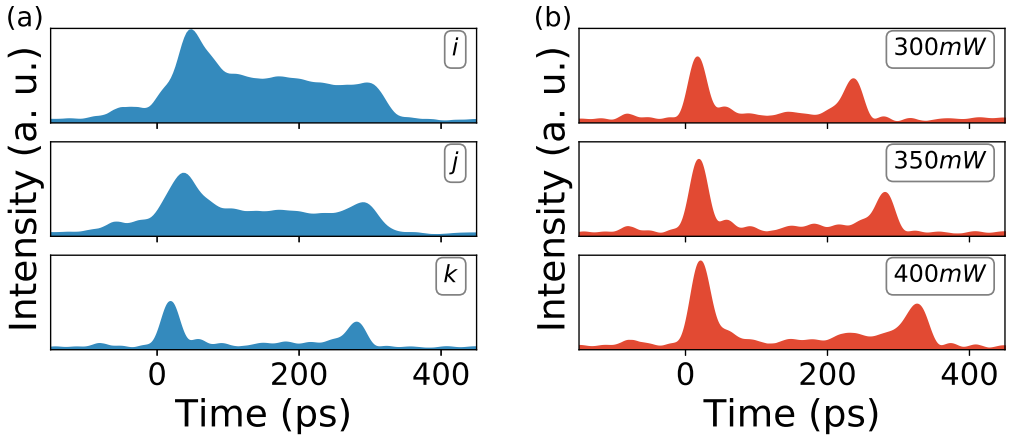

FIG. 3. (a) Oscilloscope traces of pulse after the analyzer, *i, j, k* represent different states with continuously-rotating analyzer. (b) Oscilloscope traces of pulse after the analyzer, versus increasing pump power, with analyzer fixed at state k.

where $\Delta\psi$ is the phase shift between two components. From the Stokes parameters, the orientation angle, ϕ, of the polarization ellipse can be easily calculated as

$$\tan 2\phi = \frac{S_2}{S_1} \tag{5}$$

In Fig. 4(a), we plot the calculated resonant pulse intensity $S_0(t)$ and the phase shift $\Delta\psi(t)$ (red dash dotted), as well as orientation angle $\phi(t)$ (blue dashed) across the pulse. The phase shift of two components is nearly the same across the central plane wave and starts to change when the fronts are approached. This also applies for the orientation angle of the polarization ellipse. The normalized Stokes parameters of the pulse are also plotted on the Poincaré sphere with color mapped by $S_0(t)$ in Fig. 4(b). Note that only the part that meets $S_0(t) > 0.1$ was plotted for a more clear view. One can see from the Poincaré sphere that the resonant pulse does not acquire a single SOP. The fronts show a long trajectory on the Poincaré sphere, while the central plane wave with the highest intensity converges to one point.

As the central plane wave forms the majority of the pulse, we verified that the largest energy ratio between the resolved components was found when the pulse was resolved along the major and minor axes of the polarization ellipse of the central plane wave. We then numerically perform the same polarization test, passing the pulse through the waveplate-analyzer combination. The final fields after the analyzer, versus the rotation of the analyzer in the vicinity of the minimal energy transmission, are depicted in Fig. 4(c). This polar-

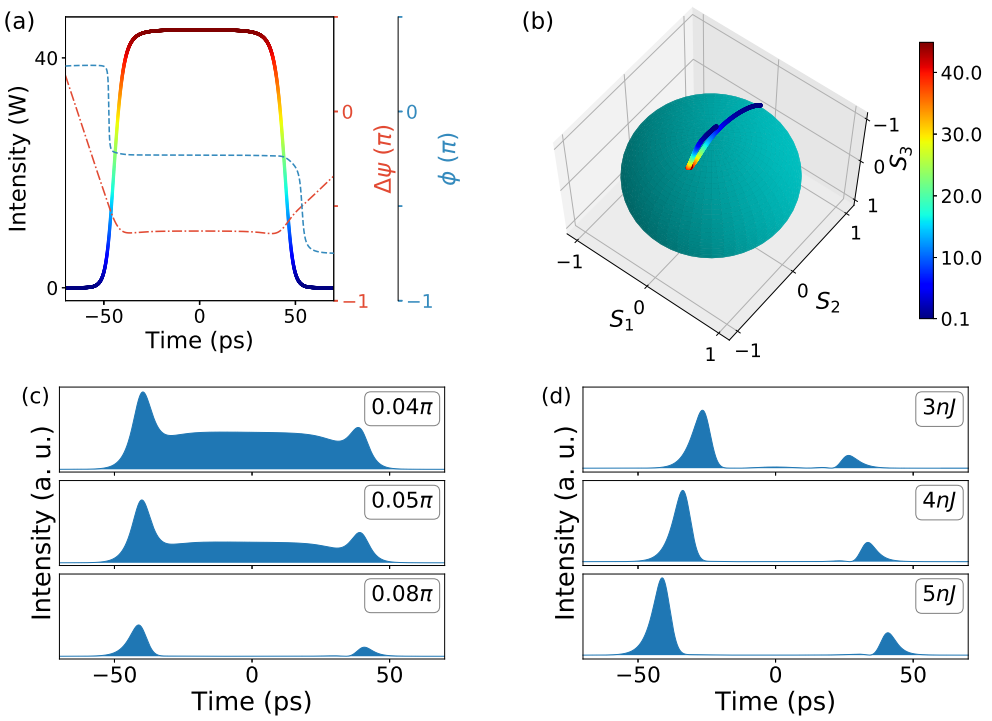

FIG. 4. Numerical results. (a) Colormap line: Calculated pulse, red dash dotted: the phase shift between its fast and slow components, blue dashed: orientation angle across the pulse. (b) Trajectory on the Poincaré sphere, of light field that meets $S_0(t) > 0.1$, color mapped by $S_0(t)$. (c) Simulated pulse profiles after the analyzer versus rotating transmission axis. (d) Simulated pulse profiles after the analyzer versus increasing E_{sat}.

ization non-conformity between fronts and the plane wave is maintained with varying gain settings, as shown in Fig. 4(d). Comparing with the experiments in Fig. 3, the simulations show good agreement.

The simulation confirms the experiment. We believe that the fiber segment connecting the output coupler and the fiber collimator does not contribute to the distinct internal polarization distribution of the DSR pulse, for two reasons. Firstly, the length of this fiber segment is less then 1 m, and from the measured output energy and pulse width, the estimated pulse peak power is about 17.4 W. Considering such a short fiber segment and the low peak power, this fiber segment would have a negligible nonlinear polarization rotating (NPR) effect on the pulse; this was then proved numerically. Secondly, the NPR effect is intensity-dependent. Intensities of the leading and trailing fronts of the original pulse are very close [see Fig. 2(a)]. However, the two fronts, after passing through the

waveplate-analyzer, exhibit significant differences (see Fig. 3). Therefore, we believe that the DSR pulse acquires this internal polarization distribution within the mode-locked fiber laser. Meanwhile, the polarization states of the two fronts are asymmetric and are found to be dependent on the cavity birefringence. For example, in the case presented, the intensity of the leading front after the waveplate-analyzer was always higher than that of the trailing front. Experimentally, by rotating the intracavity PCs, different states could be observed where the trailing front was higher. This is also confirmed in the simulation, by simply changing the polarization parameter of the fiber.

In conclusion, we have observed vector DSR pulses in a mode-locked fiber laser. The DSR pulse is a complex of two interacting dissipative fronts and a central plane wave. Utilizing that, we are able to gain insight into the internal polarization dynamics across a resonant DS. Experimental results show that the DSR pulses do not acquire a single SOP. Although the central plane wave of the pulse acquires nearly a single fixed polarization state, the dissipative fronts feature spatially-varying polarization states. Also, changes of gain condition do not affect the internal polarization dynamics. Numerical simulations confirmed the experimental observations. Despite the polarization non-conformity between fronts and the plane wave, the DSR pulses are highly stable in the laser, suggesting that the composite balance between nonlinearity, dispersion and energy exchange forms a strong attractor in dissipative systems. The experimental and theoretical analysis gives important new insight into the internal dynamics of DSs.

Key Research Program of Natural Science of Jiangsu Higher Education Institutions (17KJA416004); National Natural Science Foundation of China (NSFC) (11674133, 11711530208, 61575089, 61405079); Royal Society (IE161214); Jiangsu Province Science Foundation (BK20140231); Key Laboratory of Optoelectronic Devices and Systems of Ministry of Education and Guangdong Province (GD201705); Priority Academic Program Development of Jiangsu higher education institutions (PAPD). D. Li thanks N. Akhmediev, A. Ankiewicz and W. Chang for fruitful discussions.

* zhaoluming@jsnu.edu.cn

[1] N. Akhmediev and A. Ankiewicz, eds., *Dissipative Solitons: From Optics to Biology and*

Medicine (Springer Berlin Heidelberg, 2008).

[2] P. Grelu and N. Akhmediev, Nature Photonics **6**, 84 (2012).

[3] N. Akhmediev, J. M. Soto-Crespo, and P. Grelu, Physics Letters A **372**, 3124 (2008).

[4] G. Semaan, F. B. Braham, J. Fourmont, M. Salhi, F. Bahloul, and F. Sanchez, Opt. Lett. **41**, 4767 (2016).

[5] E. Ding, P. Grelu, and J. N. Kutz, Optics Letters **36**, 1146 (2011).

[6] D. Li, D. Tang, L. Zhao, and D. Shen, Journal of Lightwave Technology **33**, 3781 (2015).

[7] D. Li, L. Li, J. Zhou, L. Zhao, D. Tang, and D. Shen, Scientific Reports **6**, 23631 (2016).

[8] C. Cuadrado-Laborde, I. Armas-Rivera, A. Carrascosa, E. A. Kuzin, G. Beltrán-Pérez, A. Díez, and M. V. Andrés, Optics Letters **41**, 5704 (2016).

[9] Y. Barad and Y. Silberberg, Physical Review Letters **78**, 3290 (1997).

[10] S. T. Cundiff, B. C. Collings, N. N. Akhmediev, J. M. Soto-Crespo, K. Bergman, and W. H. Knox, Phys. Rev. Lett. **82**, 3988 (1999).

[11] D. Y. Tang, H. Zhang, L. M. Zhao, and X. Wu, Physical Review Letters **101**, 153904 (2008).

[12] Z.-C. Luo, Q.-Y. Ning, H.-L. Mo, H. Cui, J. Liu, L.-J. Wu, A.-P. Luo, and W.-C. Xu, Optics Express **21**, 10199 (2013).

[13] S. V. Sergeyev, C. Mou, E. G. Turitsyna, A. Rozhin, S. K. Turitsyn, and K. Blow, Light: Science & Applications **3**, e131 (2014).

[14] C. Mou, S. V. Sergeyev, A. G. Rozhin, and S. K. Turitsyn, Opt. Express **21**, 26868 (2013).

[15] X.-W. Zheng, Z.-C. Luo, H. Liu, N. Zhao, Q.-Y. Ning, M. Liu, X.-H. Feng, X.-B. Xing, A.-P. Luo, and W.-C. Xu, Applied Physics Express **7**, 042701 (2014).

[16] J. Liu, Y. Chen, P. Tang, C. Xu, C. Zhao, H. Zhang, and S. Wen, Opt. Express **23**, 6418 (2015).

[17] N. J. Doran and D. Wood, Opt. Lett. **13**, 56 (1988).